A 450-Year Perspective on California Precipitation "Flips" ✐

Eugene R. Wahl,[a,f] Andrew Hoell,[b] Eduardo Zorita,[c] Edward Gille,[a,d] and Henry F. Diaz[e]

[a] NOAA/National Centers for Environmental Information/Center for Weather and Climate/Products Branch, Boulder, Colorado;
[b] NOAA/Physical Sciences Laboratory, Boulder, Colorado; [c] Institute of Coastal Research, Helmholtz Zentrum Geesthacht,
Geesthacht, Germany; [d] Cooperative Institute for Research in Environmental Sciences, University of Colorado, Boulder, Colorado;
[e] University of Hawai'i at Mānoa, Honolulu, Hawaii

ABSTRACT: Year-to-year extreme alterations in California (CA) precipitation, denoted here as flips, present significant challenges to resource managers, emergency management officials, and the state's economy and ecosystems generally. We evaluate regional (north, central, and south) and statewide flip behavior since 1571 CE utilizing instrumental data and paleoclimate reconstructions. Flips, defined as dry-to-wet and wet-to-dry consecutive alterations between the tailward 30th percentiles of the precipitation distribution, have occurred throughout this period without indication of systematic change through the recent time of modern anthropogenic forcing. Statewide "grand flips" are notably absent between 1892 and 1957; bootstrap Monte Carlo analysis indicates that this feature is consistent with random behavior. Composites for northeastern Pacific Ocean winter sea level pressure and jet-stream winds associated with flip events indicate anomalous high or low pressure during the core precipitation delivery season for dry or wet flip years, respectively, and jet-stream conditions that are also like those associated with individual dry or wet years. Equatorial Pacific sea surface temperatures play a partial role in both dry-to-wet and wet-to-dry events in central and southern CA in the longer-period reconstruction data, with response restricted primarily to southern CA in the smaller sample-size instrumental data. Knowledge of a prior year extreme, potentially representing initiation of a flip, provides no enhancement of prediction quality for the second year beyond that achievable from skillful seasonal prediction of equatorial Pacific sea surface temperatures. Overall, results indicate that the first-order nature of flip behavior from the later 1500s reflects the quasi–white noise nature of precipitation variability in CA, influenced secondarily by equatorial Pacific sea surface conditions, particularly in southern CA.

KEYWORDS: Atmospheric circulation; ENSO; Precipitation; Paleoclimate; Data assimilation; Climate variability

1. Introduction

Intrinsic natural variability of precipitation along the west coast of North America and California (CA) in particular shows a distinct tendency of strong alternating periods of high and low precipitation (Dettinger et al. 1998; Dettinger 2013; Wang et al. 2017). Annual-scale precipitation extremes in CA often lead to socioeconomic hardship; for example, precipitation extremes of the opposite sign in subsequent years can force CA to cope with the effects of both drought and flooding simultaneously (Brown 2017). The 2012–15 drought, which cost an estimated $2.7 billion in 2015 (Howitt et al. 2015), was likely the most extreme in a millennium in terms of soil moisture deficits for the combined central and south regions of the state (Griffin and Anchukaitis 2014; regions are outlined in Fig. 1). Similarly, it was likely the most arid in terms of precipitation delivery itself since at least 1571 for the South Coast and southern Central Valley subregions (Wahl et al. 2017). The extreme wet 2017 water year (WY; from October 2016 through

September 2017, fourth wettest of 124 years in the instrumental record; NCEI 2020) relieved some immediate effects of the previous 4-yr drought, but also led to widespread flooding and threatened dam safety (Vano et al. 2018; White et al. 2019), costing an additional estimated $1.6 billion in damage (NCEI 2019). Water year 2017 was followed immediately during the first quarter of the very dry WY 2018 by devastating fires in chaparral, oak woodlands, and mixed hardwood and conifer forests in northern and southern CA, highlighting how wet-to-dry flips in particular can lead to extensive fuel buildup that is then quickly dried out and subject to catastrophic fire events (of both natural and human-caused ignition), particularly when coupled with high winds and high temperatures (Wahl et al. 2019). Water year 2018, the 14th driest in the instrumental record, was followed in turn by the very wet WY 2019, the 21st wettest (NCEI 2020).

In light of the socioeconomic and ecological costs of year-to-year precipitation extremes of the opposite sign over CA—referred to hereafter as "flips," dry-to-wet (DW) or wet-to-dry (WD)—we probe their characteristics and relationships with potentially predictable phenomena like El Niño–Southern Oscillation (ENSO), and whether they have become more prevalent in recent time concomitant with anthropogenic effects on weather and climate. We examine these questions using spatially resolved (0.5° × 0.5°) instrumental data coupled with a same-gridded reconstruction of CA WY_t (from October$_{t-1}$ through September$_t$) precipitation going back to 1571, which has been well validated and used for other evaluations of CA climate

---

[f] Retired.

Corresponding author: Eugene Wahl, generwahl@yahoo.com
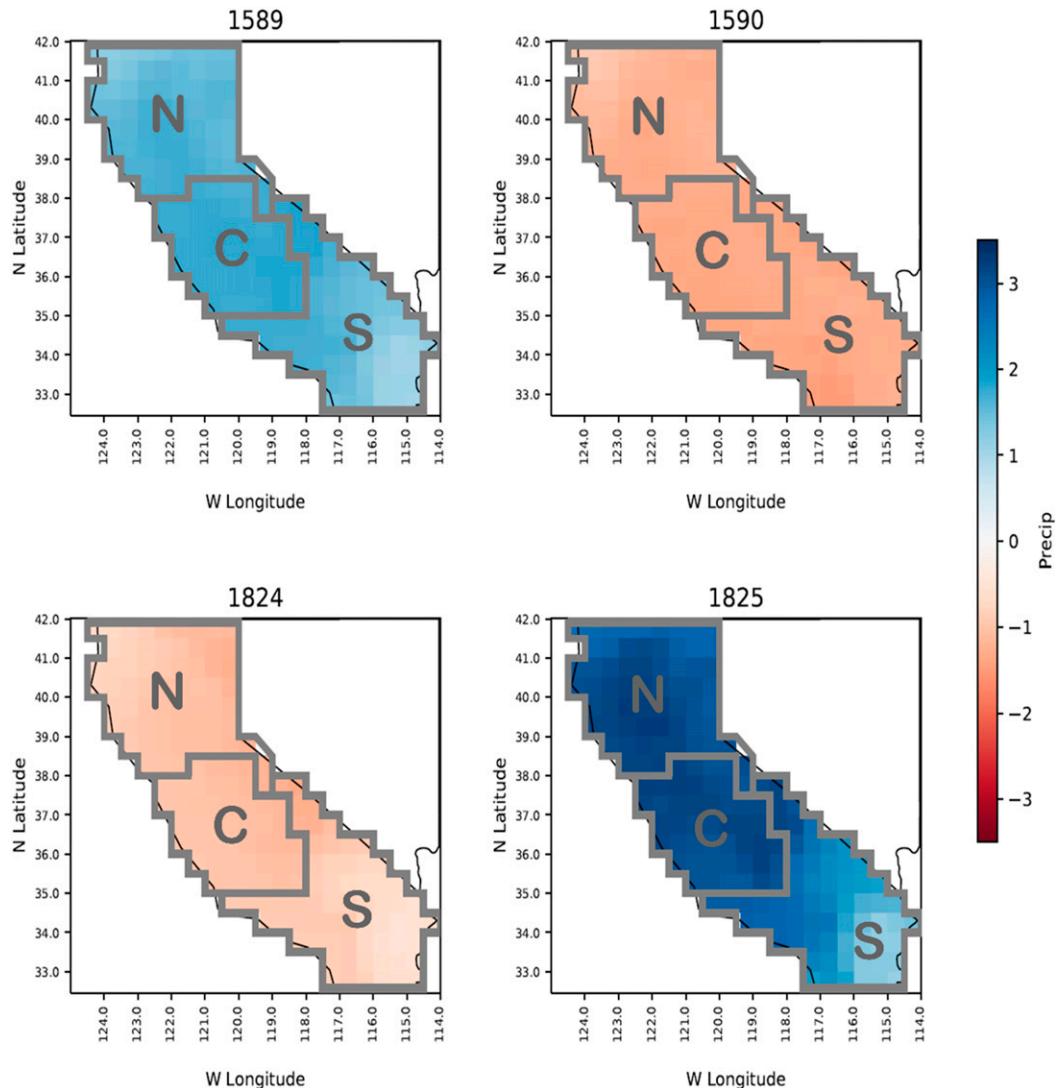
FIG. 1. Examples of CA precipitation flips from one water year to the next: (top) wet-to-dry (WD) grand flip (see section 2) between 1589 and 1590 and (bottom) dry-to-wet (DW) grand flip between 1824 and 1825, from spatially explicit reconstructions of precipitation. Values are reported as standardized anomalies, referenced to the full reconstruction period 1571–1977 (Wahl et al. 2017). Grid cells (0.5° × 0.5°) included in the North (N), Central (C), and South (S) regions are indicated. The N region encompasses climate divisions 1–3 defined by NOAA; the C region encompasses divisions 4 and 5; and the S region encompasses divisions 6 and 7 (see Wahl et al. 2017).

and climate–fire relationships (Diaz and Wahl 2015; Wahl et al. 2017, 2019). We first evaluate variability and flip behavior across the north (N), central (C), and south (S) regions (Fig. 1) of the state since there is a strong moisture gradient from N (wetter) to S (drier) CA (Fig. 2; note median amounts; see Wahl et al. 2017), and also statewide flip behavior when all three regions align in terms of sign and relative magnitude for a ''grand flip.'' Second, we evaluate the associations of CA flip behavior with northeastern Pacific winter jet-stream winds (NPJ) and sea level pressure (SLP), along with equatorial Pacific sea surface temperatures (SSTs), to provide characterization of fundamental drivers of CA precipitation in a longer-term context. Third, we determine whether skillful seasonal prediction of ENSO region SSTs could be enhanced

for prediction of a concurrent WD or DW flip by incorporating knowledge that a precipitation extreme had occurred in the previous year. Fourth, we place our results in the context of simulated CA precipitation going forward through the twenty-first century, to evaluate whether continued anthropogenic forcing of the climate system is expected to alter the regional flip hydrology from that exhibited over the past ~450 years (see Swain et al. 2018).

2. Methods

a. Definition of CA precipitation flips

A flip in CA precipitation is defined as an alternation from WY_t to WY_{t+1} from either wet (W; upper 30% of the historical
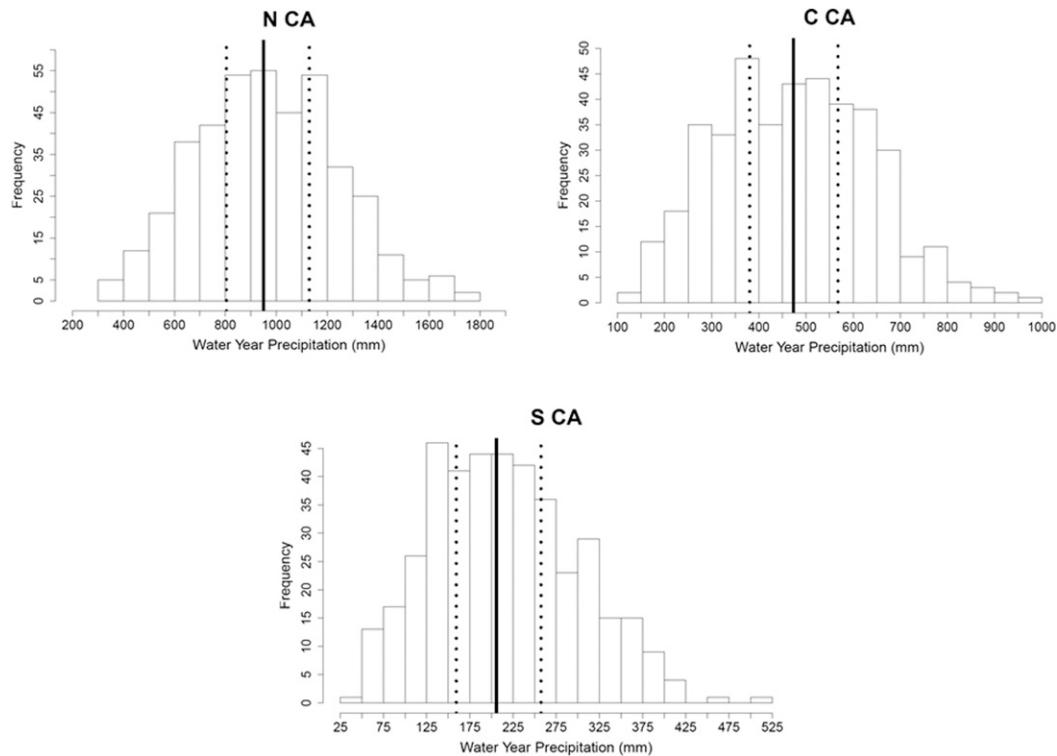
FIG. 2. Histograms of reconstructed WY precipitation (mm) for CA regions: (top left) N CA, (top right) C CA, and (bottom) S CA. Solid lines indicate the median for each region; dotted lines indicate the 30th and 70th percentiles, respectively, from left to right. Sequential DW flip years are defined as being in the lowest 30% (dry) and highest 30% (wet); the opposite sequence is defined for WD flips.

distribution) to dry (D; lower 30% of the historical distribution) or vice versa. Flips were evaluated for the nonoverlapping reconstruction (RECON; 1571–1895) and instrumental (INST; 1896–2015) periods. Flips are considered at four spatial scales: the N, C, and S regions of CA and grand flips (all three regions simultaneously). The 30th-percentile thresholds were chosen to be like the upper, lower, and middle tercile definitions used in hydroclimate evaluations and seasonal forecasts, but they isolate the extremes somewhat more distinctly while yet allowing for relatively large sample sizes over the combined reconstruction and instrumental periods. We explored using the upper and lower 20% of the distribution to define flip conditions (see Swain et al. 2018), but this resulted in a strong reduction of flip events that was especially severe for grand flip occurrences. Figure 2 indicates the nature of these stratifications in terms of the distributional representation for each of the CA regions.

b. CA precipitation reconstruction

The CA WY precipitation reconstructions were developed using the truncated-EOF principal components (PC) spatial regression (TEOF-PCSR) method described in Diaz and Wahl (2015) and Wahl et al. (2017). Primary evaluation of reconstruction characteristics and skill is also reported in those papers. Additional information about development and usage of the TEOF-PCSR method in western North America is provided in Wahl and Smerdon (2012); see Cook et al. (1994) for exposition of the fundamental method. INST data are a 0.5° × 0.5° gridding of U.S. National Oceanic and Atmospheric Administration (NOAA) spatial precipitation data for CA (NCEI 2020).

We note that tree ring data were not directly incorporated in the spatial precipitation reconstruction, but rather existing streamflow reconstructions in the western United States were incorporated as predictors, which themselves are based on tree ring data. The motivation and usage of this method has been described in detail in Diaz and Wahl (2015; see that article's associated online supplemental material for the streamflow reconstructions used) and Wahl et al. (2017). Of note, this method sought, successfully, to eliminate a too-long memory bias found by other studies in North American, European, and Asian precipitation reconstructions based directly on raw tree ring data (Bunde et al. 2013). An alternative test of the reconstruction using PCs of tree ring data directly as predictors was evaluated, which did not show validation skill to reconstruct spatial precipitation patterns (Diaz and Wahl 2015). The reconstruction begins in 1571 because of limitations in the number of streamflow predictors that extended before this time, which significantly reduced skill when evaluated with the more limited predictor set back to the fourteenth century.

MINIMIZATION OF BIAS IN IDENTIFICATION OF DW AND WD FLIPS

The spatially explicit reconstruction reported and used in Wahl et al. (2017), hereafter called 2017-RECON, is the expected-value (EV) reconstruction from the TEOF-PCSR method. For use in the analysis of CA precipitation flips, we

have developed a corrected version of 2017-RECON, since it showed an asymmetry in DW versus WD events that was determined to represent a bias relative to both INST and theoretical probability distributions, which do not exhibit such asymmetry. This feature arises as an unanticipated result from the otherwise well-performing residual errors in 2017-RECON (see Diaz and Wahl 2015; Wahl et al. 2017; Fig. S2.1 in the online supplemental material) when the reconstruction is used to extend beyond the evaluations in those articles to sequentially 1) stratify high and low precipitation extremes, 2) identify year-to-year DW or WD flips in each region based on these stratifications, and finally 3) identify simultaneous coherence across all three regional flips to make grand flips. The identification of the bias is reported in section 2 of the online supplemental material (SM). Here we document the manner in which we have corrected for it.

First, we note that in 2017-RECON, the variance of each grid cell's reconstruction was adjusted to correspond to that of INST over the calibration period. This adjustment, whose original application was to compare the extent of the 2012–15 CA drought with other dry extremes over the past ~450 years, was done to ensure that the amplitude of precipitation variability was properly captured by 2017-RECON. Our judgment is that a parallel reasoning applies here for flip evaluation. To ensure that the variance adjustment, per se, was not the cause of the regional flips asymmetry and associated false positive DW grand flips described in SM section 2, we first compared the variance-restored (2017-RECON) and non-variance-restored reconstructions, which showed nearly identical DW/WD ratios. We also inverted 2017-RECON so that it was right-skewed (or high value–skewed); as expected, the asymmetry was exactly reversed, with overly high WD/DW ratios.

Associated with 2017-RECON, a probabilistic reconstruction ensemble ($n = 1000$) was additionally developed for Wahl et al. (2017). This process utilized a Monte Carlo generalization of the "bootstrapping from residuals" technique (Dixon 2006), in which the EV reconstruction residuals were statistically modeled using the Hosking simulation algorithm (Hosking 1984), and then independent random draws were derived from the modeled distribution to drive generation of the ensemble members by repeating the entire TEOF-PCSR process for each member (the bootstrapping from residuals; see Li et al. 2007 and the acknowledgments section herein). From a statistical perspective and important in the current context, *this method produces an ensemble of probabilistically random, equally likely spatial climate reconstructions conditional on the predictor data* (Li et al. 2007). Details of the ensemble generation method in the spatially explicit context were originally provided in Wahl and Smerdon (2012).

Once we recognized that the 2017-RECON residual errors were causative of the DW/WD asymmetry (SM section 2), we systematically evaluated the associated probabilistic ensemble to determine if there was a subset of its members that could provide a way to minimize these effects. This is the case, and it provides an asymmetry-rectified version of the reconstruction, hereafter called 2020-RECON, described as follows.

The primary way to create the 2020-RECON was to search the ensemble for members in which all three regions have relatively high p values for the DW/WD ratio relative to a binomial "fair coin" model over the pre-INST reconstruction period (1571–1895), indicating low or no asymmetry. Two such thresholds were evaluated, $p = 0.25$ ($n = 48$) and $p = 0.30$ ($n = 21$), which yielded nearly identical results in terms of asymmetry reduction. We therefore chose the former threshold since the number of ensemble members in this subset is more than twice as large to form a composite. The characteristics of 2020-RECON are highly similar to 2017-RECON, with the exception of the regional and grand flip asymmetry characteristics: DW/WD ratios are 32/29, 36/32, and 34/26, for the N, C, and S regions respectively, with 13/13 grand flips. We note that although S CA still has a relatively high ratio in comparison with the even (1:1) theoretical expectation reported in SM section 2, the difference between the regional DW and WD flips lies within 1 SD overlap of the respective theoretical ranges reported there. Otherwise, the 2020-RECON and 2017-RECON reconstructions possess highly similar time series (Figs. S2.2 and S2.3 in the online supplemental material), correlating at 0.99, 0.98, and 0.97 for the N, C, and S regions respectively, and they also share highly similar autocorrelation and persistence characteristics (Figs. S2.4–S2.7 in the online supplemental material) along with similar skewness. Perhaps most important, both 2017-RECON and 2020-RECON possess Durbin–Watson values for the residual errors extremely close to 2 for all regions (1.93, 1.99, and 1.94 for the N, C, and S regions respectively in 2020-RECON, testing for negative first-order autocorrelation and robustly nonindicative of such autocorrelation; see SM section 2 for 2017-RECON values). We note that negative autocorrelation in residuals is the form that would be involved in systematic erroneous flip representation, indicating that errors on the high (low) side of the actual value for one year would be systematically associated with errors on the low (high) side in the following year (see also SM section 2).

We emphasize this latter characteristic as important, demonstrating that the presence or relative absence of flip asymmetry, and subsequent impacts on grand flips, is an isolatable feature of residual error randomness, per se, while leaving the other characteristics of the reconstruction virtually unchanged. Therefore, our assessment is that the nature of flip asymmetry can appropriately be considered a decidable characteristic for use in subsequent analysis; and since DW/WD asymmetry is indicated by both the INST data and theoretical distributions not to be a climatological feature of CA precipitation, it is further appropriate to employ the 2020-RECON for analysis of the behavior of CA flips during the reconstruction period.

To additionally confirm this logic, we also evaluated the polar opposite reconstruction subset from 2020-RECON, formed as the composite of the $n = 48$ ensemble members with the most asymmetric DW/WD flips across the three regions over 1571–1895 (37/27, 41/29, and 36/23 for the N, C, and S regions respectively, and 21/10 grand flips). This reconstruction is again very highly correlated with 2017-RECON (0.98, 0.99, and 0.99 for the N, C, and S regions respectively), and again shares with it highly similar autocorrelation and persistence characteristics, along with similar skewness. As with 2017-RECON and 2020-RECON, it possesses Durbin–Watson values of the residual errors close to 2 for all regions (1.90, 2.34, and 2.12 for the N, C, and S regions respectively, testing for negative first-order autocorrelation), again robustly nonindicative of such

autocorrelation. The singularly meaningful distinction between this highest-asymmetry reconstruction subset and its opposite end-member 2020-RECON, and of both of them with 2017-RECON, is the way in which random reconstruction errors either contribute to, or dampen, flip asymmetry. Therefore, we assess that it is logically and scientifically justified to use 2020-RECON over 1571–1895 for the more complex use-case of flip and grand flip analysis, in conjunction with INST for the post-1895 period.

c. SLP, NPJ, and SST reconstructions

The winter$_t$ [from December$_{t-1}$ to February$_t$ (DJF)] SLP and NPJ reconstructions were derived from the analog assimilation (AA) method, as described in Diaz et al. (2016) and Wahl et al. (2019) and their supplemental information. Skill evaluations for these reconstructions are also reported there [see, in particular, online supplemental Figs. S5 and S6 and associated discussion in Wahl et al. (2019)]. Additional information about the AA method can be found in Schenk and Zorita (2012) and Graham et al. (2007). The essential aspects of this method are summarized here in SM section 3, specific to the SLP and NPJ reconstructions, and below we describe how they are implemented for the Pacific SST reconstructions.

The equatorial Pacific boreal winter (DJF) SST reconstruction used here for the first time represents a new, separate application of the AA method, employing the same predictor fields in the AA process as described in SM section 3 for the SLP and NPJ reconstructions. As noted there, while the AA method in principle reconstructs large-scale (even global) 2D and 3D fields of climate variables of interest, actual reconstruction skill will be spatially heterogeneous and generally focused in the regions and variables that are most strongly climatologically related to the predictor variables. In this case, the dynamical relationship of boreal winter (DJF) equatorial Pacific SSTs with cool season moisture delivery in the American Southwest [important for summer (JJA) soil moisture in that region; St. George et al. 2010] and February–March (FM) temperature conditions in temperate western North America (Wahl et al. 2014) is utilized for the SST reconstruction.

In contrast to reconstruction methods in which a first step is the training of a statistical model linking proxy records and observations, the AA reconstruction method does not employ observations of the target variable (here SSTs). As noted in SM section 3, the reconstructed product is essentially the result of a resampling from a climate simulation, dictated by the similarity between the simulated predictors (temperate western North American FM temperature and U.S. Southwest JJA soil moisture) and the corresponding gridded reconstructions. Since no instrumental SST data are used in this setup, the concept of an out-of-training-sample validation is not applicable and the estimation of independent validation skill is instead accomplished directly by comparing the reconstructed SST field with a record of instrumental SST (here the HadISST dataset; Rayner et al. 2003). As with SLP and NPJ, we use correlation and the coefficient of efficiency (Cook et al. 1994) for quantitative comparison.

In terms of correlation, the validation skill of the SST reconstruction is generally good throughout the Niño-3 and -4 areas, and from southern Hawaii to the Pacific margin of western temperate North America (Fig. S1 in the online supplemental material). The highest values of interannual

correlation in the period 1930–80 are on the order of 0.6–0.7, and in the Niño-3 and -4 regions they are consistent with those reported for an independent Kalman filter (KF) assimilation reconstruction (Steiger et al. 2018). The correlation values are somewhat higher in these specific areas for the recently released KF assimilation reconstructions of Tardif et al. (2019), albeit for the related but not identical 2-m air temperature variable (Cayan 1980), while the validation strength away from the immediate tropical Pacific is not as strong as that reported here (Fig. S1). In terms of the coefficient of efficiency, the AA reconstruction shows validation skill in the equatorial Pacific and northwest of Hawaii, with the highest values (up to ~0.35) in the eastern portion of the Niño-4 region (Fig. S1). The AA-developed SSTs are employed here to ensure physical consistency among the far-field circulation and SST reconstructions used for analysis of potential relationships with CA precipitation flip behavior.

The Niño-4 SST region (5°N–5°S, 160°E–150°W) was utilized for evaluation of the composite relationship of ENSO behavior with flip occurrences, and thereby the potential for enhanced flip predictability. Niño-4 showed the strongest relationship with CA flip occurrences in this regard, relative to the Niño-3.4 region (5°–5°S, 170°–120° W) and to a mixed definition by type of wet or dry polarity, Niño-3 (5°N–5°S, 150°–90°W) for wet and Niño-4 for dry. Although the SST validation values of correlation skill are reasonably high and comparable to other reconstructions, they are lower in other areas of the tropical and North Pacific, and the values of the coefficient of efficiency indicate skill according to that metric in the eastern portion of the Niño-4 region but not throughout it. These skill characteristics are to some extent expected given that the North American predictor fields are constrained regionally and northeastern Pacific SLP and NPJ are more directly related to the predictor fields than are tropical Pacific SSTs. However, noting that the statistical link between the AA reconstructed Niño-4 SSTs and the first-order independent CA precipitation reconstruction (see SM section 3) is very similar to the link derived from instrumental SSTs and instrumental precipitation (Fig. S15 in the online supplemental material), we consider the SST reconstruction to be reasonable to employ in this context of regional study of CA precipitation.[1]

---

[1] We note additionally that the coefficient-of-efficiency metric is considered to be difficult to pass as an indicator of validation skill (Cook et al. 1994) and has been demonstrated to lead to potential false negative interpretations of the quality of paleoclimate reconstructions in some circumstances, such as the patterns of important historically documented droughts in China (Wahl and Morrill 2010; Cook et al. 2010; see the latter article's online supplemental material). Relatedly, in simulation tests using long paleoclimate model output, the relatively short independent validation windows that are possible during the instrumental period of record have been shown to possess a general tendency toward overly conservative interpretations of reconstruction skill relative to centuries-long validation periods that are possible in the simulation environment (Mann et al. 2007; a caveat is that this outcome is potentially constrained to the simulation context). These considerations additionally suggest that it is reasonable to use the SST reconstruction in the current context.
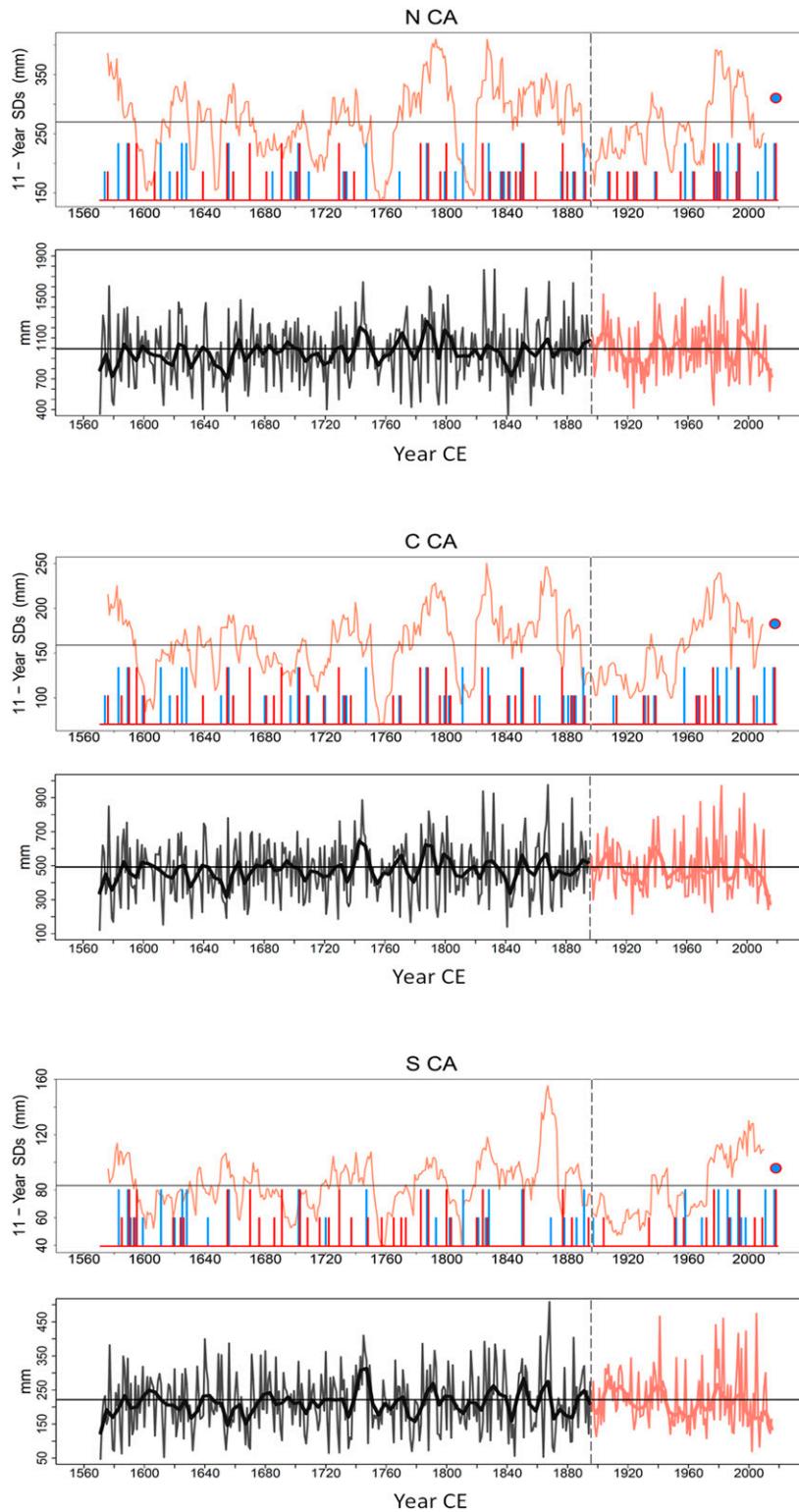
FIG. 3. Regional CA precipitation (mm) flips with running 11-yr precipitation standard deviations and precipitation time series. Sections indicate the (top) N, (middle) C, and (bottom) S regions. In the top panel of each section, short red bars indicate region-specific DW events and short blue bars indicate WD events; tall bars indicate grand flips entraining all three regions, following the same color scheme; salmon-colored continuous time series

3. Results

a. Flip characteristics

Time series of the flips for each region and CA-wide grand flips are shown in Fig. 3, along with the 11-yr running standard deviations (SDs) of precipitation for each region (upper panel of each section). Figure 3 also shows the regional precipitation time series for comparison (lower panel of each section). Both DW and WD flips have been a consistent occurrence of regional and statewide precipitation over the entire period examined, without indication of systematic increase or decrease through the period of modern anthropogenic forcing impact—defined here as since 1900 (IPCC 2014, see Fig. SPM.1 therein)—including the most recent grand flips in WYs 2017–19. [See Wahl et al. (2017) for additional discussion of CA climatological precipitation deficits in relation to the amplification of droughts by anthropogenic temperature forcing.] This characteristic, along with some clustering of events and nonflip episodes, is expectable in light of the white noise–like behavior CA precipitation exhibits over the full period we examine (Figs. S2.4–S2.7 in the online supplemental material; Wahl et al. 2017; Diaz and Wahl 2015). Flip occurrences are not systematically related with overall variability; flips and nonflips occur in periods of both low and high variability. Notable examples include the DW flip in S CA starting in 1757, during the lowest 11-yr running variability for that region, and the longest period of very high variability in C CA that occurred between 1863–73, during which no flips occurred (Fig. 3). [We note that the SD time series in Fig. 3 are centered on their midyear and thus are directly comparable to flip timing.]

The 11-yr running SDs of precipitation indicate a period of relatively enhanced variability since ~1970 in all three regions, but this variability is not unprecedented over the past half-millennium (Fig. 3). Notable earlier peaks in variability in N and C CA occur in the 1570s to early 1580s, the late 1700s to early 1800s, and the 1820s to 1830s; and in C and S CA in the 1860s to 1870s. These results remain generally unchanged when the running SD length is increased to 15 and 21 years (Figs. S3 and S4 in the online supplemental material), with the addition that C CA matches its earlier maxima in the 1970s to 1980s at the 15- and 21-yr lengths (Figs. S3 and S4). Most recently, variability has declined in all three regions at these time lengths (Fig. 3; see also online supplemental Figs. S2–S4) but remains at or near a secondary high in S CA at the 11–21-yr lengths.

A particularly notable feature of the flips time series is the long "hiatus" of grand flips between 1892 and 1957 (Fig. 3), which we highlight by evaluating running sums of the grand flips (both DW and WD) as shown in Fig. 4 for 51-yr running periods. The running sum value is continuously ≤ 1 between 1903 and 1951 and goes to 0 between 1917 and 1932, periods for such low values that have no parallel either before or after the early twentieth century. The hiatus follows after a previous high in the decade of the 1800s and precedes a similar high at the current end of the time series and is driven by reductions in flips in C (and especially) S CA during this time. In this case, the reduced number of C CA flips is associated with corresponding periods of low, but not lowest, variability at the 11-, 15-, and 21-yr time scales (and similar for S CA at the 11-yr scale) (Fig. 3) and online supplemental Figs. S3 and S4), and absolutely lowest variability at the 15- and 21-yr scales in S CA (Figs. S3 and S4). The profile of the running sum data in Fig. 4 could be considered suggestive of a possible ~200-yr period for the high and relatively low values of the grand flips. We evaluated this possibility quantitatively with a wavelet analysis (not shown), which does indicate power at ~200 yr^{-1} frequency since the later 1700s, but not earlier. Since that span of time represents essentially one "wavelength" of such a quasi-periodicity, we assess that it represents too little information to pursue such a hypothesized detection further.

Considering the singular nature of the grand flip hiatus in our observed record in conjunction with the white noise–like character of CA precipitation, the question arises whether such an event is rare enough to reject a null hypothesis that it is consistent with random occurrence. If so, then the further question would arise as to its potential cause. To evaluate the question of rareness probabilistically, we developed a Monte Carlo bootstrap analysis ($n = 1000$), randomizing the sequence of years and determining the regional and grand flip occurrences for each random iteration, then in turn replicating the running sum trajectory as in Fig. 4. Nearly 30% of the iterations (297 of 1000, an estimated $p = 0.297$) exhibit hiatuses of equal or greater length and equal or greater depth than the observed grand flip hiatus. Thus, while this analysis identifies the observed hiatus as a probabilistically unusual event, it plausibly could be a manifestation of the random variability that characterizes CA precipitation more generally, falling well short of rejecting a null hypothesis of random occurrence at typical significance thresholds (defined here as $p \leq 0.2$).

Looking to the future, model simulations indicate CA is in an uncertain transition zone between ongoing midlatitude increases and subtropical decreases in precipitation (Chang et al. 2015), in conjunction with regional heterogeneity in projected

←

indicate running 11-yr standard deviations (SDs) of the region's precipitation. The bottom panel of each section shows corresponding regional precipitation time series: gray represents reconstruction from 1571 to 1895; salmon represents instrumental values from 1896 onward; thick lines represent approximately decadal lowess smoothing. Horizontal solid lines indicate mean values of time series (11-yr running SDs in the top panels and instrumental precipitation in the bottom panels); vertical dashed lines indicate the end of reconstructed values at 1895 and start of instrumental values at 1896. Running SD and precipitation time series end in 2015 to remain independent of the most recent flip behavior: grand flips for WYs 2017–18 (WD) and 2018–19 (DW), denoted by blue–red dots.
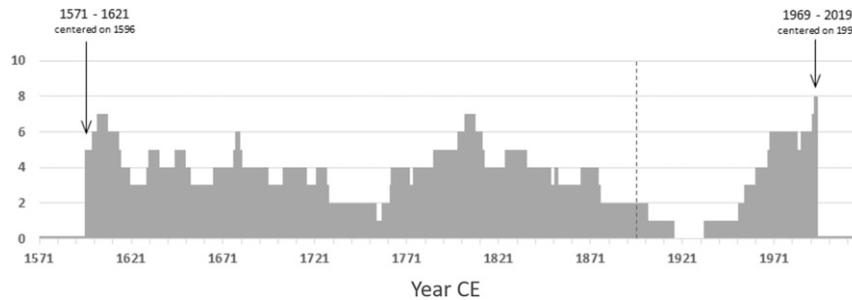
FIG. 4. The 51-yr running sums of both DW and WD statewide grand flips. The vertical dashed line indicates the end of reconstructed annual values at 1895 and start of instrumental annual values at 1896. Grand flips of WYs 2017–2018 (WD) and 2018–19 (DW) are included (see Fig. 3).

shifts of midlatitude jet steam activity (Simpson et al. 2016). Even considering these uncertainties, recent future evaluations suggest that while CA is expected to receive the same or slightly more annual precipitation on average, this increase will be accompanied by greater variability (Berg and Hall 2015; Pierce et al. 2018), particularly in S CA, and in turn a large increase in DW flip events (Swain et al. 2018; note that these authors denote DW flips as "whiplash" events). Dynamically, this increase in DW events is driven by a reduction in typical wet season storms in conjunction with more and more short, intense atmospheric river events (Gershunov et al. 2019). If they occur, such changes would represent a fundamental shift in the nature of CA precipitation, especially in S CA, from the white noise–like character we find—and concomitant large but plausibly random features such as long grand flip hiatuses—to a more fundamentally forced regime.

b. Northeastern Pacific circulation conditions and Pacific SSTs associated with flips

Composites of winter SLP and NPJ for DW and WD flips are shown in Figs. 5–7, using the SLP and NPJ reconstructions described in SM section 3 (covering the period 1571–1980). Parallel composites for Pacific SSTs are shown in Figs. 8 and 9 for the SST reconstructions described in section 2c. Corresponding composites for SLP and NPJ using the Twentieth Century Reanalysis data, v.2c (Compo et al. 2011; Slivinski et al. 2019) and for SSTs using the HadISST data (Rayner et al. 2003) are shown in Figs. S9–S13 in the online supplemental material (covering 1930–2013 for SLP and NPJ and 1930–2015 for SSTs).

The reconstruction regional flip composites conform with known features associated with wet and dry conditions in CA. SLP conditions show anomalous low pressure/anomalous ridging in the northeastern Pacific and adjacent western North America for wet/dry conditions (Figs. 5 and 6; see Wahl et al. 2019, online supplemental Fig. S1 therein). NPJ conditions show 1) enhanced maximum velocity and a narrowed, southward-shifted latitudinal range of highest velocities along the American west coast during wet years for zonal (u-component) winds, with reduced zonal velocity and a widened, northward-shifted latitudinal range of highest velocities (for C and S CA) during dry years; and 2) enhanced/more negative meridional (v component) velocity during dry extremes,

corresponding to more northerly flow of the blocking high-pressure ridge (Fig. 7; see Wahl et al. 2019, Figs. 1 and 2 therein). We note that these NPJ composite relationships are strongly like those associated with low (high) fire years in CA (Wahl et al. 2019, Fig. 2 therein), corresponding with those shown here for wet (dry) years, respectively. For C and S CA, wet or dry years are significantly associated with anomalously warm or cool SSTs, respectively, in the equatorial region and some surrounding eastern areas, whereas these relationships are much weaker and mostly nonsignificant for N CA with the exception of the eastern equatorial region for year$_{t+1}$ of WD events (Figs. 8 and 9; see Dettinger et al. 1998). Grand flip associations resemble those for the regional flips, but with stronger SLP ridging and more extensively cool central Pacific SSTs for dry years, coupled with a lack of spatial significance for warm central Pacific SSTs during wet years related to the smaller sample sizes involved compared to the regional flip composites (Figs. S5–S8 in the online supplemental material).

The reanalysis-based circulation composites exhibit similar characteristics to their reconstruction counterparts, but with reduced amplitude (SLP) and reduced strength of anomaly significance (both SLP and NPJ) (Figs. S9–S11 in the online supplemental material). For the SLP composites, these features are particularly notable in all three regions for DW year$_t$ (Fig. S9) and in C CA for WD year$_t$ (Fig. S10), and they are notable generally for the NPJ composites (Fig. S11). As with the grand flips, the much reduced sample sizes compared to the reconstruction composites can make significance more difficult to attain. It is also possible that the circulation variability involved is differentially captured by the reanalysis data compared to the SLP and NPJ reconstructions—that is, that the model states selected to form reconstructions in the AA method are relatively less variable in terms of their circulation behavior associated with CA wet and dry extremes.

The instrumental-derived SST composites are less like their reconstruction counterparts for the dry-year components of both DW (year$_t$) and WD (year$_{t+1}$) flips in N and C CA. In these cases, nonsignificant neutral-to-small positive anomalies predominate in much of the equatorial Pacific and surrounding regions, with some nonsignificant cool anomalies in the eastern equatorial area for N CA in DW year$_t$ and C CA in WD year$_{t+1}$, along with cool anomalies in the western equatorial
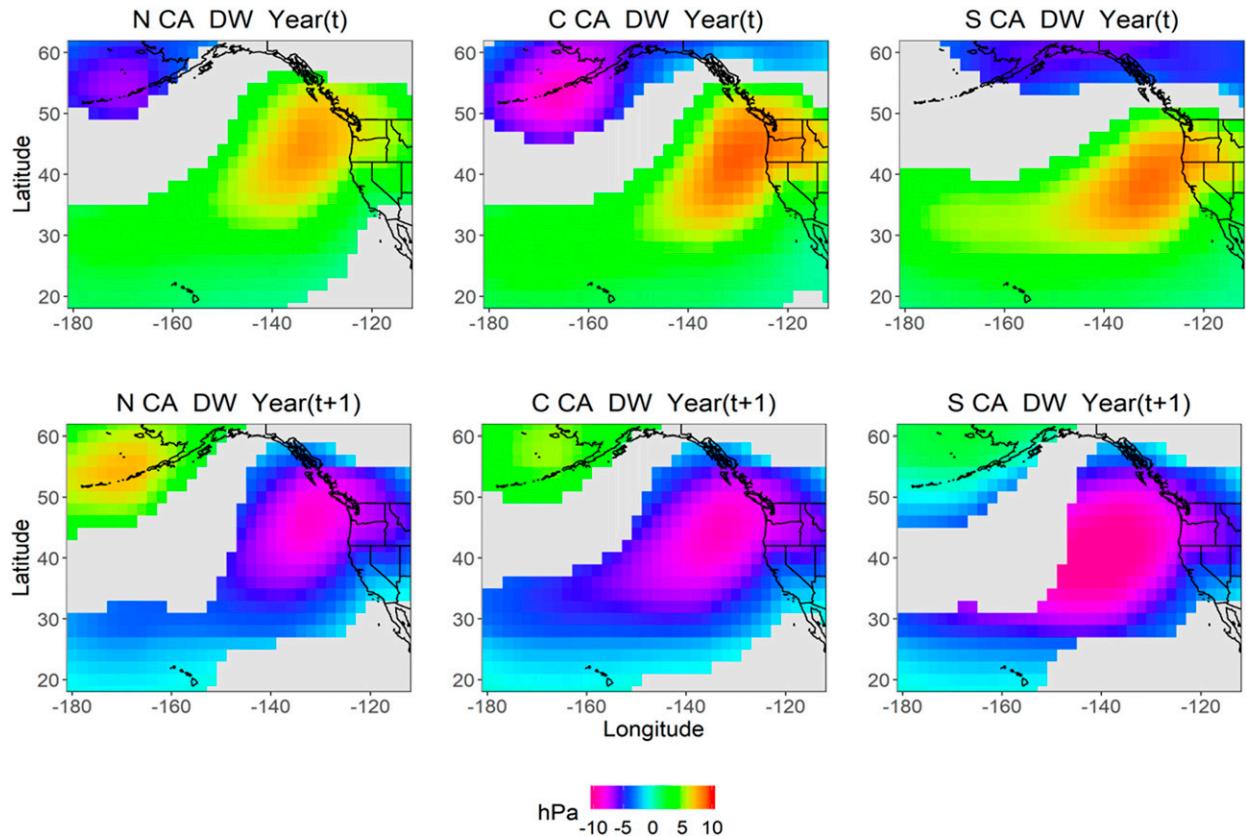
FIG. 5. Northeast Pacific reconstructed winter SLP composite anomalies for CA DW precipitation flips: (top) year$_t$ and (bottom) year$_{t+1}$ for the (left) N, (center) C, and (right) S regions; Coloring (nongray regions) indicates significance ($p \leq 0.10$), estimated using a two-sample t test with inhomogeneous variances (comparing flip composite values with nonflip averages). The time period is 1571–1980; seasonality is DJF.

area for both N (some significant) and C CA (nonsignificant) in DW year$_t$ (Figs. S12 and S13 in the online supplemental material). The S CA DW year$_t$ composite exhibits nonsignificant cool anomalies in the central equatorial Pacific along with nonsignificant neutral-to-small positive anomalies elsewhere in the equatorial region (Fig. S12); in WD year$_{t+1}$, extensive but nonsignificant cool anomalies predominate in the equatorial Pacific for S CA (Fig. S13). The wet-year composites are a mixture of nonsignificant warm and cool anomalies in the equatorial Pacific and surrounding regions for N and C CA in WD year$_t$ and nonsignificant positive values for N CA in DW year$_{t+1}$. For S CA, the wet-year composites for both DW (year$_{t+1}$) and WD (year$_t$) flips exhibit strong, significant positive anomalies through much of the equatorial Pacific and surrounding regions, similarly (but with less amplitude and extent of spatial significance) for C CA in DW year$_{t+1}$. The lack of significance and nonconformance of N CA and C CA (for the D component generally and year$_t$ of WD flips) with a S CA-type composite is a feature of the weakening of the relationship between equatorial Pacific SSTs and CA precipitation from south to north, as this relationship progresses toward a reverse polarity (especially for cool La Niña–like conditions) in the American Pacific Northwest (Schonher and Nicholson

1989; Dettinger et al. 1998). The reconstruction SST composites reflect this weakening for N CA (and to a limited degree for C CA), but retain the overall sign relationship of wet/dry CA precipitation with warm/cool equatorial Pacific SSTs that is only clearly exhibited for S CA in the instrumental SST data, in particular for the association of wet conditions with El Niño (EN)-like warm SST anomalies. As with the reanalysis flip composites for SLP and NPJ, the reduced sample sizes compared to the reconstruction composites may play a role in these differences. Compared to the circulation cases, there also may be an enhanced likelihood that the model states selected to form Pacific SST reconstructions in the AA method exhibit relatively more specificity/less variability in relation to CA wet and dry extremes. We discuss this consideration further in section 4b.

c. Flips conditioned by ENSO and potential for enhancement of prediction skill for flip occurrences

Following on the Pacific SST results outlined in section 3b above, we additionally evaluated the relationship of CA precipitation flips with ENSO behavior in a more formal and quantitative way, focusing on the Niño-4 region as noted in section 2c.
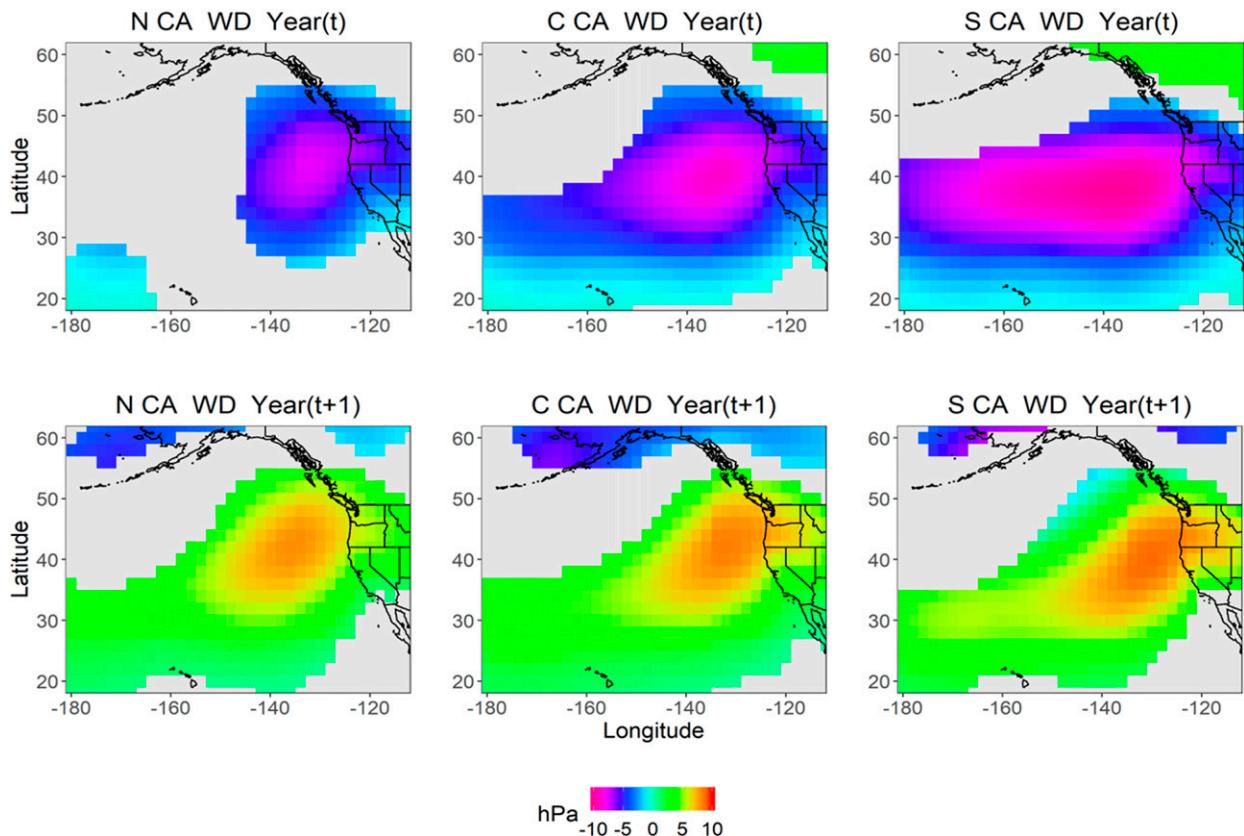
FIG. 6. As in Fig. 5, but for WD precipitation flip events.

Two-way histograms of reconstructed winter Niño-4 anomaly values for DW and WD flips are shown in Fig. 10, for all three regions and grand flips. If Niño-4 SSTs were perfectly explanatory of CA precipitation, and by inclusion of flip behavior for a ''canonical'' CA (especially S CA) ENSO response, the histogram values would be entirely located in the lower-right quadrant of each panel for DW flips (Fig. 10, top-left section), with < 0 La Niña (LN)-like anomalies for year_t and > 0 EN-like anomalies for year_{t+1}. Conversely, the histogram values would be entirely located in the upper-left quadrant of each panel for WD flips (Fig. 10, top-right section), with > 0 EN-like anomalies for year_t and < 0 LN-like anomalies for year_{t+1}.

As anticipated from the more general results described in section 3b, the two-way histogram outcomes indicate that, for the DW case, flips in S CA (Fig. 10, top-left section, lower-right panel) are most closely related with ENSO, with 40% of events occurring in the lower-right quadrant. S CA also shows the greatest, and similar, specificity for the WD case (Fig. 10, top-right section, lower-right panel), with ~43% of events occurring in the upper-left quadrant. DW flips in C CA are slightly less strongly related with Niño-4 SSTs (Fig. 10, top-left section, lower-left panel) with ~36% of events occurring in the lower-right quadrant, and similarly for WD events (Fig. 10, top-right section, lower-left panel) with ~38% of events occurring in the upper-left quadrant. These percentages are approximately 2

times the reconstruction-based empirical likelihood of a flip occurrence, which is ~19% [see He and Sheffield (2020), who find that DW flips occur ~11% of the time globally at the end of drought periods]. We note in this context Webb et al. (2003), who find a similar enhancement ratio for S CA in instrumental observations—in their analysis, for EN relative to the climatological chance of a wet year in that region. DW flips in N CA are more evenly related with Niño-4 SSTs (Fig. 10, top-left section, upper-right panel), with ~24% of events occurring in the lower-right quadrant and ~29% of WD events (Fig. 10, top-right section, upper-right panel) occurring in the upper-left quadrant. Grand flips show strength similar to that in S and C CA: ~43% in the lower-right quadrant for DW events (Fig. 10, top-left section, upper-left panel) and ~36% in the upper-left quadrant for WD events (Fig. 10, top-right section, upper-left panel).

Corresponding results for *all* 2-yr sequences are shown in the bottom section of Fig. 10. These results do not cluster in either the lower-right or upper-left quadrants, highlighting the role ENSO plays in S and C CA flip sequences. To place this comparative evaluation in a probabilistic context, we performed a separate Monte Carlo bootstrap analysis ($n = 1000$), randomizing the sequence of years and corresponding SST values and determining the all-year two-way histogram results for each random iteration. This analysis indicates that the percentages noted for S and C CA and for grand flips are
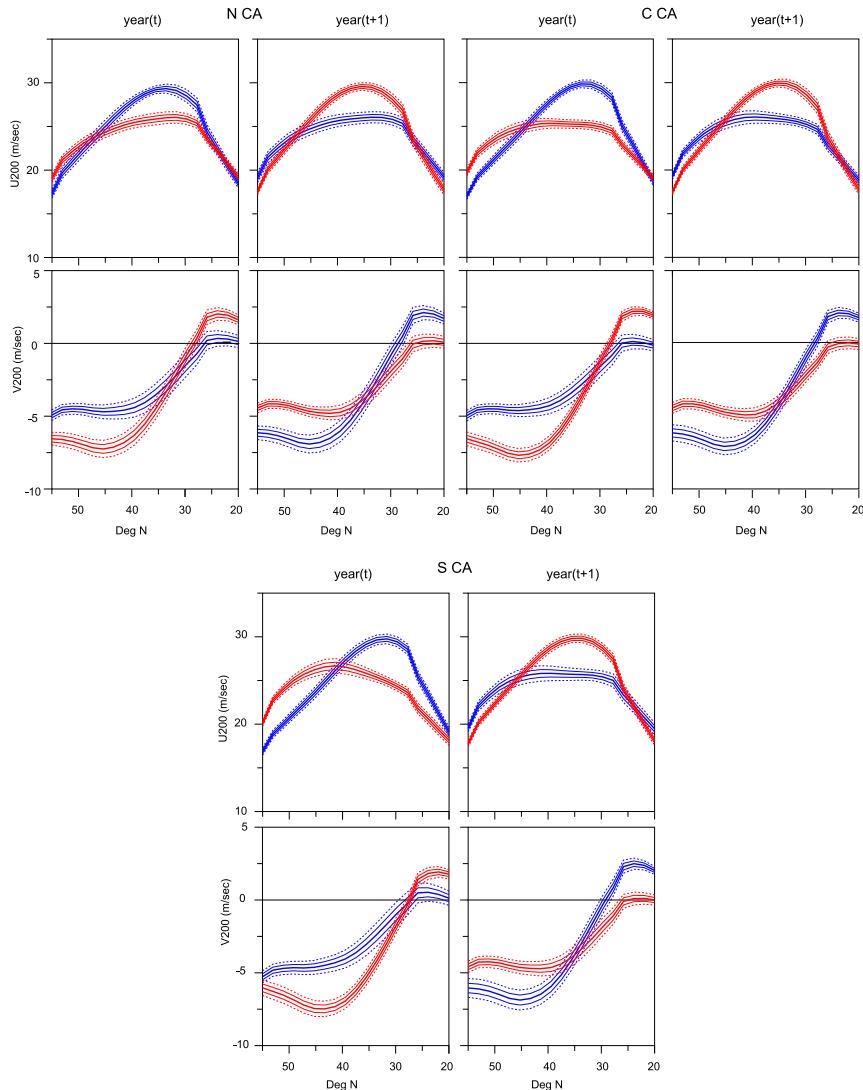
FIG. 7. Coastal Northeast Pacific reconstructed winter NPJ composites for CA precipitation flips. Sections indicate the (top left) N, (top right) C, and (bottom) S regions. In each section, the left panels show year$_t$ and the right panels show year$_{t+1}$ latitudinal profiles of 200-hPa u-wind velocity averaged between 120° and 130°W in the top panels and 200-hPa v-wind velocity averaged between 110° and 120°W in the bottom panels. Longitudinal windows represent areas with the highest correlation between CA precipitation and NPJ u and v components (Wahl et al. 2019). Red color indicates DW flips, and blue color indicates WD flips, as in Fig. 3; thin solid lines and dashed lines indicate ±1 and ±2 sample-estimated standard error of the mean (SEM), respectively. The time period is 1571–1980; seasonality is DJF.

strongly significant (estimated $p \ll 0.01$), and the N CA WD percentage is also significant at the estimated $p < 0.01$ level. The N CA DW percentage is not significant at any commonly used significance level (as above, defined to be $p \leq 0.2$). A parallel Monte Carlo bootstrap for *nonflip* years (i.e., omitting the years in which a flip in either direction is initiated) yields the same results. We note that the bootstrap analyses we use rest, in part, on the approximately white noise nature of CA precipitation (Figs. S2.4–S2.7 in the online supplemental material), motivating the appropriateness of randomizing the

sequence of years [see Wahl et al. (2017), where this reasoning was relatedly applied].

It is important to consider that these observed relationships between (especially) S and C CA flips and Niño-4, while estimated to be highly statistically significant, indicate that ENSO's role is still at most partial in terms of flip behavior. None of the percentages observed represent even half of the DW or WD flip events. Additionally, and again as expected, a more muted response occurs (except for S CA for DW events, with ~44% in the lower-right quadrant) using the smaller-sample-size
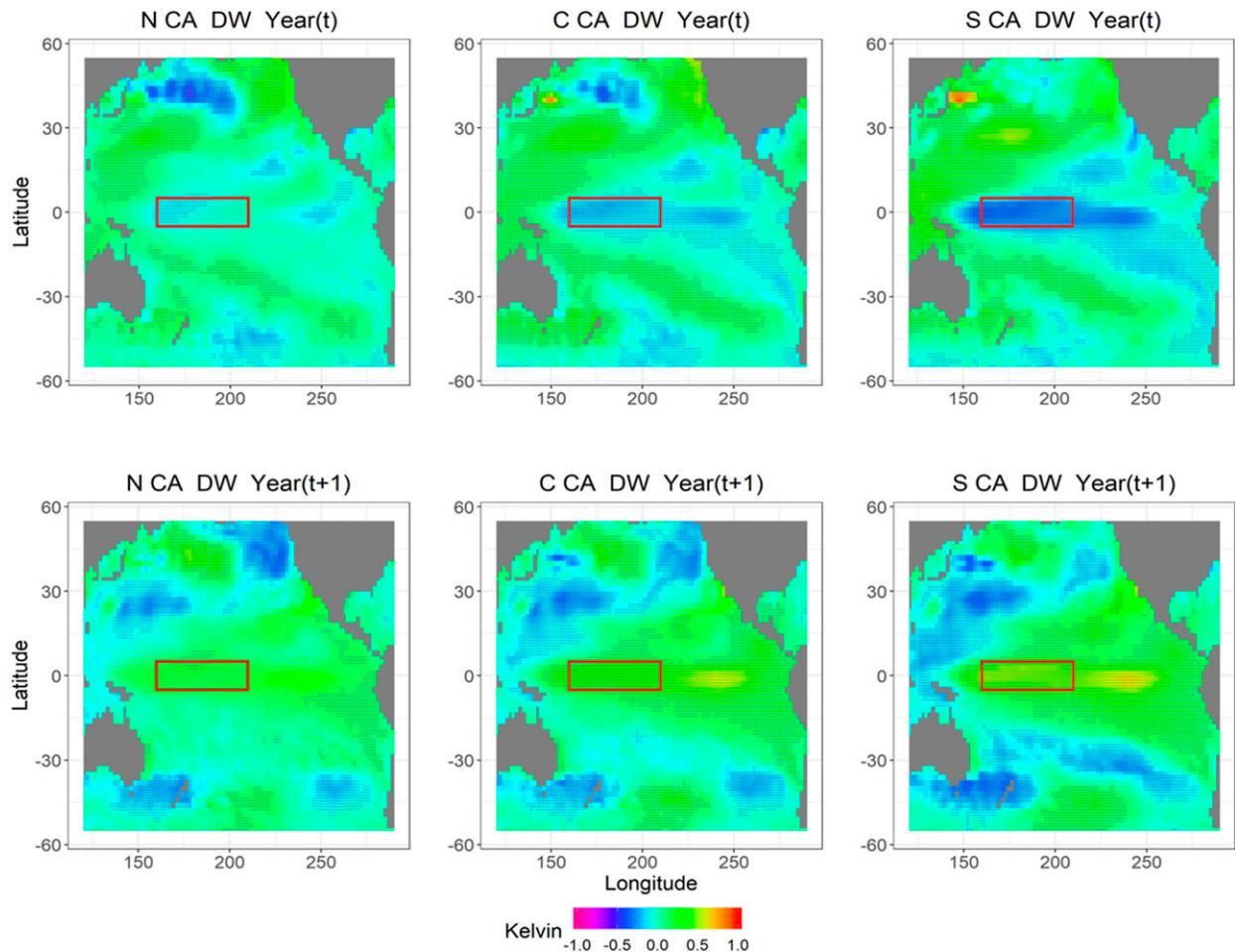
FIG. 8. Pacific Ocean reconstructed boreal winter SST composite anomalies for CA DW precipitation flips; (top) year$_t$ and (bottom) year$_{t+1}$ for the (left) N, (center) C, and (right) S regions; The red box outlines the Niño-4 area (see section 2c and online supplemental Fig. S1 for skill characteristics of the Niño-4 area). Stippling indicates significance ($p \leq 0.10$), estimated using a two-sample t test with inhomogeneous variances (comparing flip composite values with nonflip averages). The time period is 1571–1980; seasonality is DJF.

instrumental SST data (Fig. S14 in the online supplemental material, top panels). This caution is particularly important in the context of evaluating the potential for enhancing forecast skill of flip occurrences. The question at interest in this context is whether prior knowledge that a potential flip initiation year (a potential year$_t$) has occurred can enhance skill when coupled with a skillful prediction of year$_{t+1}$ ENSO area SST conditions (evaluated here as Niño-4). In this regard, we note that in instrumental data since 1950 wet conditions occur for S CA when there is an EN ~46% of the time (Climate.gov 2019), and this information is *not* conditioned on year$_t$ dry conditions. Therefore, even in the best identified case of DW flips in S CA (considering both the reconstruction and instrumental data outcomes), our results indicate no potential for enhancement of flip prediction capability for year$_{t+1}$, based on skillful prediction of year$_{t+1}$ ENSO area SST conditions *in conjunction with* knowledge that a potential flip initiation year had occurred in year$_t$. Continued development of prediction skill for ENSO-related SSTs thus remains as a key goal for enhancing

early management adaptation to the possibility of a flip. This outcome is considered further in section 4 below.

4. Summary and discussion

a. Summary

As outlined in the introduction, we have addressed three important aspects of year-to-year extreme flips of CA precipitation. These aspects are summarized as follows.

1) First, and most fundamental, we have examined flip occurrences since 1571, with the clear result that flips have occurred throughout the past ~450 years and do not exhibit systematic increase or decrease associated with enhanced anthropogenic forcing (section 3a; Fig. 3). The most notable feature of the long flips record is a hiatus of grand flips (across the entire state, N, C, and S) in the later nineteenth century and first half of the twentieth century (Fig. 4), which is statistically consistent with purely random behavior.
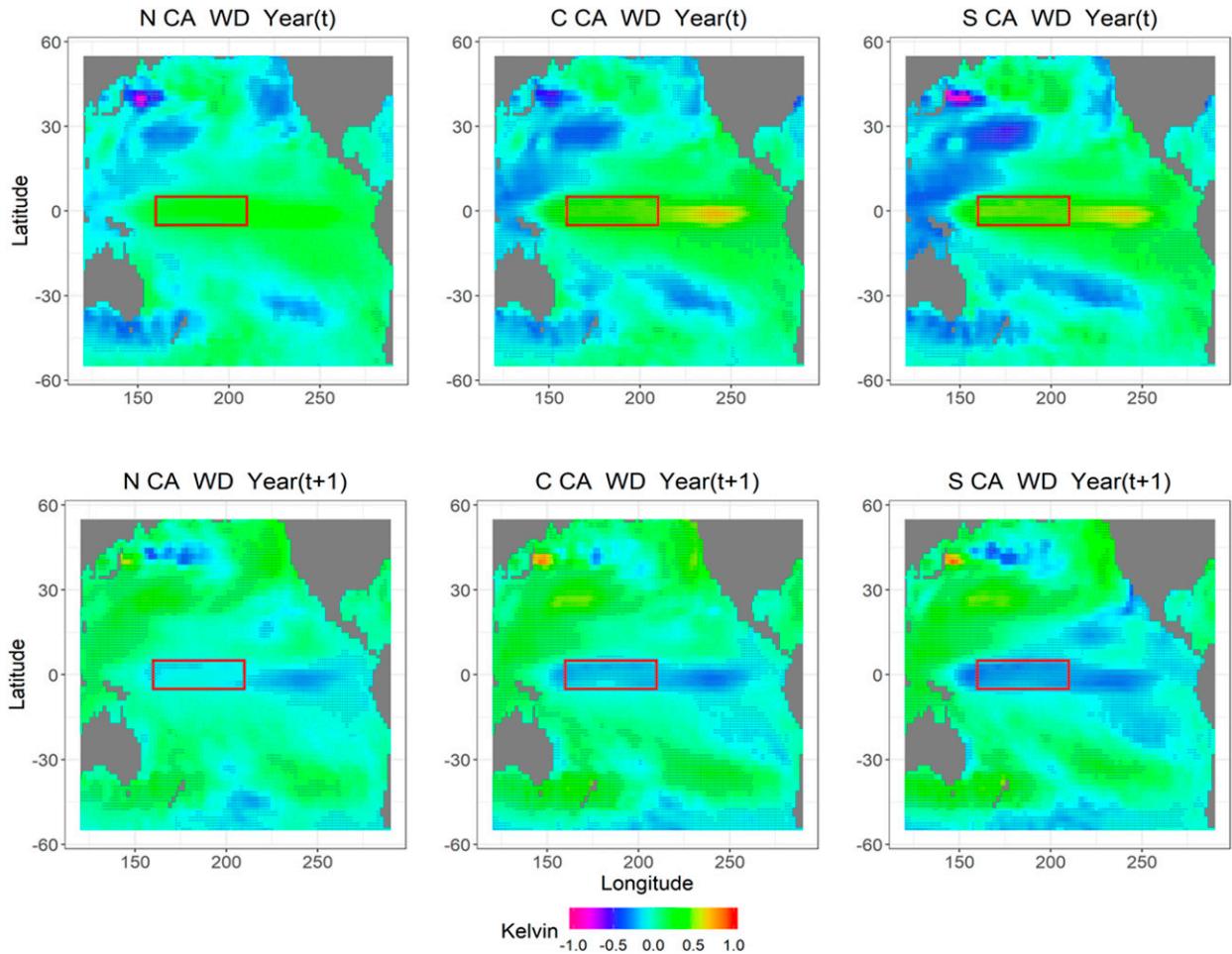
FIG. 9. As in Fig. 8, but for WD precipitation flip events.

2) Second, we have evaluated the associations for each region, and for grand flips, between flip occurrences and northeastern Pacific circulation (SLP and NPJ) and equatorial Pacific SST conditions (section 3b). Reconstruction and reanalysis composites for northeastern Pacific winter sea level pressure and jet-stream winds associated with flip events generally indicate significant anomalous high (low) pressure during the core winter precipitation delivery season for dry (wet) flip years (Figs. 5 and 6 and online supplemental Figs. S5, S9, and S10), and jet-stream conditions that are similarly like those associated with individual dry or wet years (Fig. 7 and online supplemental Figs. S6 and S11). Cool (warm) equatorial Pacific SSTs are significantly related to dry (wet) flip years in C and S CA in the longer-period reconstruction data, with weaker and largely nonsignificant relationships for N CA (Figs. 8 and 9). In the smaller sample-size instrumental data composites, significant and notably warm equatorial Pacific SSTs are associated with wet flip years in S CA (particularly in DW $year_{t+1}$), and similarly but with somewhat less amplitude and spatial extent for C CA in DW $year_{t+1}$; cool but nonsignificant SSTs are associated with the dry flip years in S CA (especially in WD $year_{t+1}$) (Figs. S12 and S13 in the online supplemental material). The other three cases for C CA and three of the four cases for N CA indicate nonsignificant mixed warm and cool equatorial Pacific SSTs or neutral-to-weak opposite sign relationships from those exhibited by the reconstruction data (Figs. S12 and S13); nonsignificant same-sign SSTs occur for N CA in DW $year_{t+1}$. We note that, along with the inherent interest these associations carry for CA climatology and resource/emergency management considerations in the state, the attempt to provide long-term quantitative understanding of circulation and teleconnected phenomena associated with fundamental temperature and hydroclimate reconstructions is a key goal of high-resolution paleoclimatology during the Common Era (see PAGES 2k Project 2020).

3) Third, we have evaluated whether there is potential for enhancement of flip prediction capability for $year_{t+1}$, based on skillful prediction of $year_{t+1}$ ENSO area SST conditions in conjunction with knowledge that a potential flip initiation year had occurred in $year_t$ (section 3c). Knowledge of a prior year extreme provides no enhancement of prediction quality for the second year ($year_{t+1}$) beyond that achievable
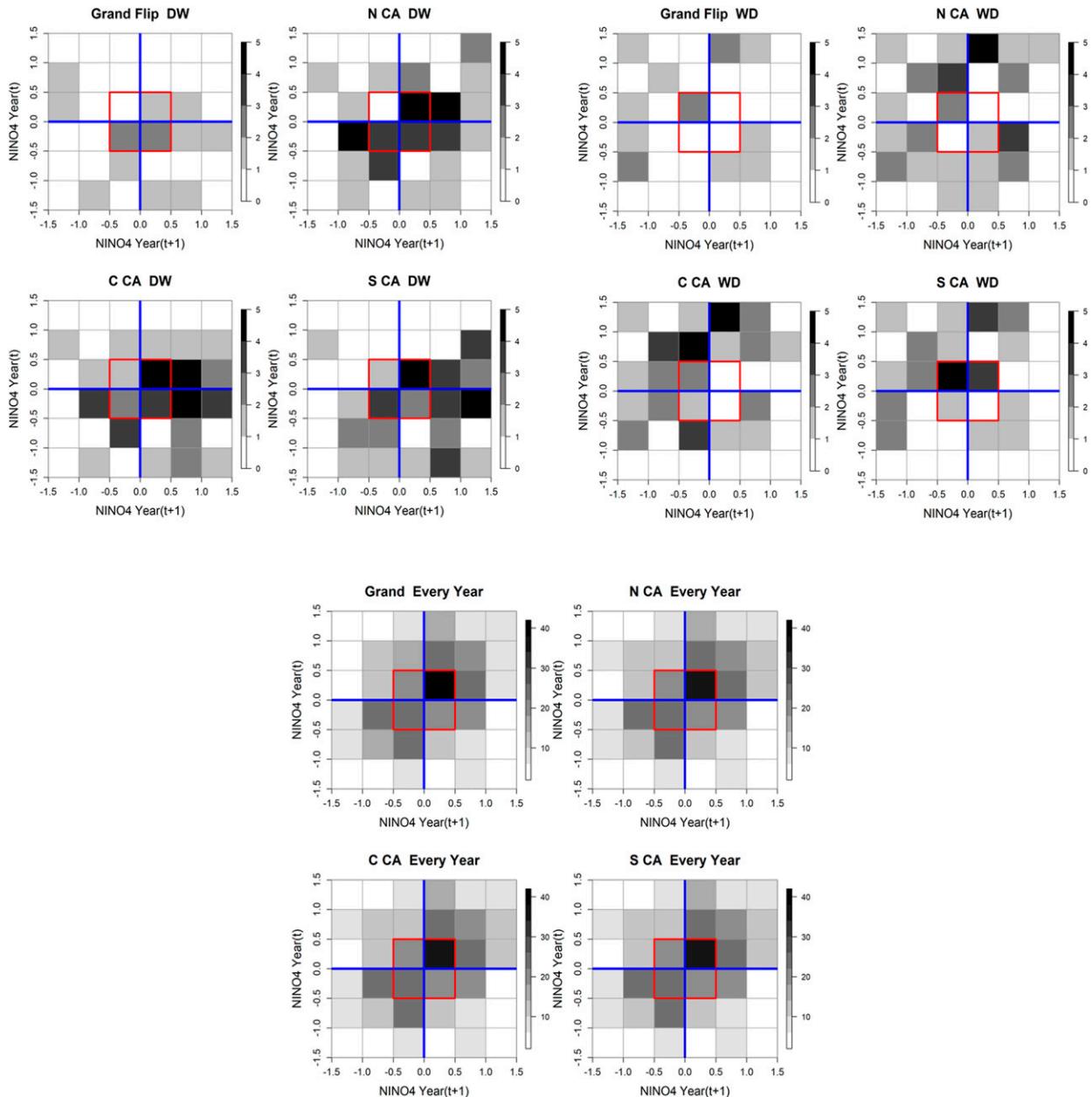
FIG. 10. Two-way histograms of reconstructed boreal winter Niño-4 SST anomaly values for CA precipitation flip years and all years. Sections indicate (top left) DW events, (top right) WD events, and (bottom) every year included. Clockwise from top left in each section, the panels show grand flips, N, S, and C regions; year$_t$ values are shown on the y axis, year$_{t+1}$ values are shown on the x axis (note difference in scale for the every-year-included case). Shading indicates frequency in each 0.5° × 0.5° histogram grid box; the red outline indicates anomaly values of ≤0.5°. The time period is 1571–1980; seasonality is DJF. (Note that all panels in the bottom section are the same since every year is included.)

from skillful seasonal prediction of equatorial Pacific SSTs (evaluated here as Niño-4 region SSTs) (see Fig. 10 and online supplemental Fig. S14).

b. Technical consideration regarding Pacific SST reconstruction by the AA method

As noted in section 3b, the lack of significance and non-conformance of N CA and C CA instrumental SSTs (for the D

component generally and year$_t$ of WD flips) with a S CA-type flip composite is a feature of the weakening of the relationship between equatorial Pacific SSTs and CA precipitation from south to north. The reconstruction SST composites also reflect this weakening for N CA (and to a limited degree for C CA), but retain the overall sign relationship of wet/dry CA precipitation with warm/cool equatorial Pacific SSTs that is only clearly exhibited for S CA in the instrumental data. While the

reduced sample size of the instrumental composites compared to their reconstruction counterparts may play a role in these differences, the model states selected to form the Pacific SST reconstruction in the AA method may exhibit inherently more specificity/less variability in relation to CA wet and dry extremes. This possible limitation of the AA method is an important area for future work for its improvement. Inclusion of additional hydroclimate predictor information from the East Asian margin of the Pacific (the Monsoon Asia Drought Atlas; Cook et al. 2010) has been attempted, but without increase in reconstruction skill of equatorial Pacific SSTs. More generally, two of the authors (EZ and EW) are initiating experiments to couple a KF postprocessing step with the AA method, with the goal to exploit the optimality properties of the Kalman filter to enhance the AA output after analog state selection, and thereby increase skill (Pfister et al. 2020). Theoretically, this extension of the AA method should allow amelioration of model deficiencies for AA reconstruction, such as those described above as potential issues in this case, contingent in part on the inherent noise/error variability of the paleo-observation data used as predictors in the AA method, which represents a fundamental limiting factor in this process.

c. Discussion

The lack of predictability enhancement reported in section 3c is generally consistent with the white noise–like character of CA precipitation time series, over the period evaluated, in both reconstruction and instrumental data (Figs. S2.4–S2.7 in the online supplemental material) as noted in section 3a (see below with regard to the future). Thus, the first-order nature of flip behavior from the later 1500s up to the present appears to be primarily the result of the quasi-random character of CA precipitation; even a feature as singular as the grand flip hiatus between 1892 and 1957 is consistent with random behavior. This first-order characteristic is influenced secondarily by ENSO SST conditions, with the greatest ENSO influence in S CA and for DW flips there. That ENSO precipitation teleconnections in CA are generally strongest for the S region is well known (e.g., NOAA 2019a,b; see Fig. S15 in the online supplemental material, right panels), and we show that this is also true in a secondary sense for year-to-year precipitation flip behavior (Figs. 8–10 and online supplemental Figs. S12–S14).

The essentially stationary character of CA flip behavior that we report during the period evaluated is consistent with the model results of Swain et al. (2018) during the twentieth and early twenty-first centuries (see Fig. 4 therein). Progressing into the future, Swain et al. (2018) find a clear trend toward greater DW flip events, particularly strongly expressed in S CA, driven by anthropogenic forcing manifesting through strong increases in subseasonal wet storm sequences (both N and S) and additionally by enhanced extreme dry seasons (especially in the S). Gershunov et al. (2019) evaluate this tendency in greater temporal detail, and conclude that increases in wet extremes will be driven almost entirely by enhanced individual atmospheric river events (see Dettinger 2013) in the context of increased occurrence of dry days, especially in shoulder seasons. Again, this combination could lead to a greater frequency of DW events.

Thus, the combination of the multicentury results presented here and model-based studies of potential future conditions suggests that anthropogenic radiative forcing is likely to significantly alter the previous long-term character of CA precipitation and flip events in the coming decades. These alterations are projected to change CA hydroclimate into an historically unprecedented, more radiatively forced condition of greater moisture extremes, with concomitant effects on both human and natural systems in one of North America's most populated areas and one of the world's most productive economic regions [see Wahl et al. (2019) for related considerations concerning fire in CA].

Data availability. The Pacific SST reconstructions are available online on publication (https://www.ncdc.noaa.gov/paleo-search/).

REFERENCES

Berg, N., and A. Hall, 2015: Increased interannual precipitation extremes over California under climate change. *J. Climate*, **28**, 6324–6334, https://doi.org/10.1175/JCLI-D-14-00624.1.

Brown, E. G., 2017: Governor Brown lifts drought emergency, retains prohibition on wasteful practices. Accessed 8 October 2019, https://www.ca.gov/archive/gov39/2017/04/07/news19747/index.html.

Bunde, A., U. Büntgen, J. Ludescher, J. Luterbacher, and H. von Storch, 2013: Is there memory in precipitation? *Nat. Climate Change*, **3**, 174–175, https://doi.org/10.1038/nclimate1830.

Cayan, D., 1980: Large-scale relationships between sea surface temperature and surface air temperature. *Mon. Wea. Rev.*, **108**, 1293–1301, https://doi.org/10.1175/1520-0493(1980)108<1293:LSRBSS>2.0.CO;2.

Chang, E. K. M., C. Zheng, P. Lanigan, A. M. W. Yau, and J. Neelin, 2015: Significant modulation of variability and projected change in California winter precipitation by extratropical cyclone activity. *Geophys. Res. Lett.*, **42**, 5983–5991, https://doi.org/10.1002/2015GL064424.

Climate.gov, 2019: U.S. winter precipitation during every El Niño since 1950. Accessed 7 October 2019, https://www.climate.gov/news-features/featured-images/us-winter-precipitation-during-every-el-ni%C3%B1o-1950.

Compo, G. P., and Coauthors, 2011: The Twentieth Century Reanalysis Project. *Quart. J. Roy. Meteor. Soc.*, **137** (654), 1–28, https://doi.org/10.1002/qj.776.

Cook, E. R., K. R. Briffa, and P. D. Jones, 1994: Spatial regression methods in dendroclimatology: A review and comparison of two techniques. *Int. J. Climatol.*, **14**, 379–402, https://doi.org/10.1002/joc.3370140404.

——, K. Anchukaitis, B. Buckley, R. D'Arrigo, G. Jacoby, and W. Wright, 2010: Asian monsoon failure and megadrought during the last millennium. *Science*, **328**, 486–489, https://doi.org/10.1126/science.1185188.

Dettinger, M. D., 2013: Atmospheric rivers as drought busters on the U.S. West coast. *J. Hydrometeor.*, **14**, 1721–1732, https://doi.org/10.1175/JHM-D-13-02.1.

——, D. R. Cayan, H. F. Diaz, and D. M. Meko, 1998: North–south precipitation patterns in western North America on interannual-to-decadal timescales. *J. Climate*, **11**, 3095–3111, https://doi.org/10.1175/1520-0442(1998)011<3095:NSPPIW>2.0.CO;2.

Diaz, H. F., and E. R. Wahl, 2015: Recent California water year precipitation deficits: A 440-year perspective. *J. Climate*, **28**, 4637–4652, https://doi.org/10.1175/JCLI-D-14-00774.1.

——, ——, E. Zorita, T. W. Giambelluca, and J. Eischeid, 2016: A five-century reconstruction of Hawaiian Islands winter rainfall. *J. Climate*, **29**, 5661–5674, https://doi.org/10.1175/JCLI-D-15-0815.1.

Dixon, P. M., 2006: Bootstrap resampling. *Encyclopedia of Environmetrics*, John Wiley and Sons.

Gershunov, A., and Coauthors, 2019: Precipitation regime change in western North America: The role of atmospheric rivers. *Sci. Rep.*, **9**, 9944, https://doi.org/10.1038/s41598-019-46169-w.

Graham, N., and Coauthors, 2007: Tropical Pacific–mid-latitude teleconnections in medieval times. *Climatic Change*, **83**, 241–285, https://doi.org/10.1007/s10584-007-9239-2.

Griffin, D., and K. J. Anchukaitis, 2014: How unusual is the 2012–2014 California drought? *Geophys. Res. Lett.*, **41**, 9017–9023, https://doi.org/10.1002/2014GL062433.

He, X. and J. Sheffield, 2020: Lagged compound occurrence of droughts and pluvials globally over the past seven decades. *Geophys. Res. Lett.*, **47**, e2020GL087924, https://doi.org/10.1029/2020GL087924.

Hosking, J. R. M., 1984: Modeling persistence in hydrological time series using fractional differencing. *Water Resour. Res.*, **20**, 1898–1908, https://doi.org/10.1029/WR020i012p01898.

Howitt, R., D. MacEwan, J. Medellín-Azuara, J. Lund, and D. Sumner, 2015: Economic analysis of the 2015 drought for California agriculture. UC Davis Center for Watershed Sciences, and ERA Economics, and UC Agricultural Issues Center Rep., 30 pp., https://watershed.ucdavis.edu/files/biblio/Final_Drought%20Report_08182015_Full_Report_WithAppendices.pdf.

IPCC, 2014: *Climate Change 2014: Synthesis Report*. R. K. Pachauri and L. A. Meyer, Eds., IPCC, 151 pp.

Li, B., D. Nychka, and C. Ammann, 2007: The "hockey stick" and the 1990s: A statistical perspective on reconstructing hemispheric temperatures. *Tellus*, **59A**, 591–598, https://doi.org/10.1111/j.1600-0870.2007.00270.x.

Mann, M., S. Rutherford, E. Wahl, and C. Ammann, 2007: Robustness of proxy-based climate field reconstruction methods. *J. Geophys. Res.*, **112**, D12109, https://doi.org/10.1029/2006JD008272.

NCEI, 2019: U.S. Billion-dollar weather and climate disasters: Table of events. NCEI, accessed 8 October 2019, https://www.ncdc.noaa.gov/billions/events/US/2010-2019.

——, 2020: Climate at a glance (for California water year precipitation). NCEI, accessed 19 April 2020, https://www.ncdc.noaa.gov/cag/statewide/time-series/4/pcp/12/9/1895-2019?base_prd=true&begbaseyear=1901&endbaseyear=2000.

NOAA, 2019a: El Niño precipitation teleconnections. Climate Prediction Center, accessed 24 July 2019, https://www.cpc.ncep.noaa.gov/products/analysis_monitoring/ensocycle/elninosfc.shtml.

——, 2019b: La Niña precipitation teleconnections. Climate Prediction Center, accessed 24 July 2019, https://www.cpc.ncep.noaa.gov/products/analysis_monitoring/ensocycle/laninasfc.shtml.

PAGES, 2020: Past Global Changes 2k Network. Accessed 19 May 2020, http://pastglobalchanges.org/science/wg/2k-network/.

Pfister, L., S. Brönnimann, M. Schwander, F. A. Isotta, P. Horton, and C. Rohr, 2020: Statistical reconstruction of daily precipitation and temperature fields in Switzerland back to 1864. *Climate Past*, **16**, 663–678, https://doi.org/10.5194/cp-16-663-2020.

Pierce, D. W., D. Cayan, and J. Kalansky, 2018: Climate, drought, and sea level rise scenarios for the Fourth California Climate Assessment. *California's Fourth Climate Change Assessment*. California Energy Commission, 71 pp.

Rayner, N. A., and Coauthors, 2003: Global analyses of sea surface temperature, sea ice, and night marine air temperature since the late nineteenth century. *J. Geophys. Res.*, **108**, 4407, https://doi.org/10.1029/2002JD002670.

Schenk, F., and E. Zorita, 2012: Reconstruction of high resolution atmospheric fields for northern Europe using analog-upscaling. *Climate Past*, **8**, 1681–1703, https://doi.org/10.5194/cp-8-1681-2012.

Schonher, T., and S. E. Nicholson, 1989: The relationship between California rainfall and ENSO events. *J. Climate*, **2**, 1258–1269, https://doi.org/10.1175/1520-0442(1989)002<1258:TRBCRA>2.0.CO;2.

Simpson, I., R. Seager, M. F. Ting, and T. Shaw, 2016: Causes of change in Northern Hemisphere winter meridional winds and regional hydroclimate. *Nat. Climate Change*, **6**, 65–70, https://doi.org/10.1038/nclimate2783.

Slivinski, L. C., and Coauthors, 2019: Towards a more reliable historical reanalysis: Improvements for version 3 of the Twentieth Century Reanalysis system. *Quart. J. Roy. Meteor. Soc.*, **145**, 2876–2908, https://doi.org/10.1002/qj.3598.

Steiger, N., J. Smerdon, E. Cook, and B. Cook, 2018: A reconstruction of global hydroclimate and dynamical variables over the Common Era. *Sci. Data*, **5**, 180086, https://doi.org/10.1038/sdata.2018.86.

St. George, S., D. Meko, and E. Cook, 2010: The seasonality of precipitation signals embedded within the North American Drought Atlas. *Holocene*, **20**, 983–988, https://doi.org/10.1177/0959683610365937.

Swain, D., B. Langenbrunner, J. D. Neelin, and A. Hall, 2018: Increasing precipitation volatility in twenty-first century California. *Nat. Climate Change*, **8**, 427–433, https://doi.org/10.1038/S41558-018-0140-Y.

Tardif, R., and Coauthors, 2019: Last Millennium Reanalysis with an expanded proxy database and seasonal proxy modeling. *Climate Past*, **15**, 1251–1273, https://doi.org/10.5194/cp-15-1251-2019.

Vano, J., M. Dettinger, R. Cifelli, D. Curtis, A. Dufour, K. Miller, J. R. Olsen, and A. Wilson, 2018: Hydroclimatic extremes as challenges for the water management community: Lessons from Oroville Dam and Hurricane Harvey [in "Explaining Extreme Events of 2017 from a Climate Perspective"]. *Bull. Amer. Meteor. Soc.*, **100**, S9–S14, https://doi.org/10.1175/BAMS-D-18-0219.1.

Wahl, E. R., and C. Morrill, 2010: Toward understanding and predicting monsoon patterns. *Science*, **328**, 437–438, https://doi.org/10.1126/science.1188926.

——, and J. Smerdon, 2012: Comparative performance of paleo-climate field and index reconstructions derived from climate proxies and noise-only predictors. *Geophys. Res. Lett.*, **39**, L06703, https://doi.org/10.1029/2012GL051086.

——, H. F. Diaz, J. E. Smerdon, and C. M. Ammann, 2014: Late winter temperature response to large tropical volcanic erup-tions in temperate western North America: Relationship to ENSO phases. *Global Planet. Change*, **122**, 238–250, https://doi.org/10.1016/j.gloplacha.2014.08.005.

——, ——, R. Vose, and W. S. Gross, 2017: Multi-century evalu-ation of recovery from strong precipitation deficits in California. *J. Climate*, **30**, 6053–6063, https://doi.org/10.1175/JCLI-D-16-0423.1.

——, E. Zorita, V. Trouet, and A. Taylor, 2019: Jet stream dy-namics, hydroclimate, and fire in California from 1600 CE to present. *Proc. Natl. Acad. Sci. USA*, **116**, 5393–5398, https://doi.org/10.1073/pnas.1815292116.

Wang, S. Y. S., J.-H. Yoon, E. Becker, and R. Gillies, 2017: California from drought to deluge. *Nat. Climate Change*, **7**, 465–468, https://doi.org/10.1038/nclimate3330.

Webb, R., J. Eischeid, H. Diaz, K. Wolter, C. Smith, and R. Dole, 2003: Global Patterns of the risk of seasonal extremes related to ENSO. *28th Annual Climate Diagnostics and Prediction Workshop*, Reno, Nevada, accessed 7 October 2019, https://www.esrl.noaa.gov/psd/people/robert.s.webb/ensorisk/precip/precip_risk.html.

White, A., B. Moore, D. Gottas, and P. Neiman, 2019: Winter storm conditions leading to excessive runoff above California's Oroville Dam during January and February 2017. *Bull. Amer. Meteor. Soc.*, **100**, 55–70, https://doi.org/10.1175/BAMS-D-18-0091.1.